Title
Three-Dimensional Numerical Simulation of Plume Downwash with a k–ϵ Turbulence Model

Journal
Journal of Applied Meteorology, 29(7)

ISSN
0894-8763

Authors
Guenther, Alex
Lamb, Brian
Stock, David

Publication Date
1990-07-01

DOI
10.1175/1520-0450(1990)029<0633:tdnsop>2.0.co;2

Three-Dimensional Numerical Simulation of Plume Downwash with a $k - \epsilon$ Turbulence Model

ALEX GUENTHER* AND BRIAN LAMB

Laboratory for Atmospheric Research, Washington State University, Pullman, Washington

DAVID STOCK

Department of Mechanical and Materials Engineering, Washington State University, Pullman, Washington

(Manuscript received 11 August 1989, in final form 13 January 1990)

ABSTRACT

Plume downwash at a large oil-gathering facility in the Prudhoe Bay, Alaska oil-field reservation was simulated in a series of numerical experiments. The purpose of this study was to investigate the potential of the numerical model as a means of assessing the impacts of pollutants emitted from buoyant sources influenced by complex aerodynamic wakes. The model is a three-dimensional, Cartesian coordinate, finite difference code that solves the nonhydrostatic, time-averaged equations for the conservation of momentum and energy. The code uses a modified form of the standard first-order, two-equation ($k - \epsilon$) engineering turbulence closure model.

Wind tunnel and field investigations of dispersion at this arctic industrial complex indicate that dispersion is significantly influenced by building-generated airflow disturbances. We have used the numerical model to simulate directly the mean features of the flow field and dispersion from a buoyant source at an industrial site. The flow features varied depending on the size, number, and orientation of the buildings. A recirculation cavity was present in all model simulations and varied from 0.8 H_B to 2 H_B (building height). This agrees closely with results of wind tunnel studies. The model simulates a velocity defect of 0.6, a factor of 3.4 increase (relative to the approach flow) in turbulent kinetic energy (k), a factor of 5 increase in dissipation of $k(\epsilon)$, and a 45% increase in turbulent viscosity at a downwind distance of 2 H_B from the building. At a downwind distance of 5 H_B, the plume rise of the simulated thermal plume decreased by 70% compared to the no-building case while the vertical and horizontal widths of the plume increased by 45% and 30%, respectively. These results generally reproduce the plume downwash and dispersion observed in wind tunnel and field investigations.

1. Introduction

Air quality simulation models provide a means of estimating current air quality and predicting the impacts of changes in pollutant emission levels. Regulatory agencies rely primarily upon Gaussian plume model calculations to provide these estimates. Gaussian models are reasonably accurate for the relatively homogeneous turbulence and unidirectional flow observed in the atmospheric boundary layer (ABL) flow over open terrain but often fail to predict concentrations accurately under conditions that deviate significantly from the assumptions required for the Gaussian model. Airflow around the clustered and interconnected buildings of an arctic oil gathering facility is an example of a situation where plume dispersion is greatly influenced by complex processes. This is especially the case for buoyant emissions from the low stacks typical of arctic industrial sources. We previously investigated dispersion near an oil gathering center (GC2) in Prudhoe Bay, Alaska with a series of wind tunnel and field experiments. Our evaluation of the performance of Gaussian models, with analytical plume downwash algorithms, indicates that the uncertainty associated with analytical dispersion model estimates at this site is greater than a factor of 2 for most cases (Guenther et al. 1989; Guenther et al. 1990).

Accurate estimates of ground-level concentration distributions in the wake of GC2, and at many other industrial facilities, require site-specific dispersion data. Wind tunnel and field investigations are presently the only reliable means of acquiring these data in the wake of an industrial complex. Recent advances in computer technology have enabled investigators to simulate three-dimensional turbulent flow around buildings using large eddy simulation (Murakami et al. 1987) and by using the $k - \epsilon$ turbulence model to close the time-averaged Navier–Stokes equations (Paterson and Alpelt 1986; Mathews 1987; Murakami and Mochida 1988). All of these studies were conducted to examine wind engineering applications requiring knowledge of ve-

* Present affiliation: Cooperative Institute for Research in Environmental Sciences UC-Boulder Box 216, Boulder CO 80309-0216.

Corresponding author address: Brian Lamb, Laboratory for Atmospheric Research, Washington State University, Pullman, WA 99164-2910.

locity, turbulent kinetic energy, and pressure fields near buildings. Murakami and Mochida (1988) compared their results with wind tunnel observations, which included velocity, pressure, and turbulent kinetic energy measurements, and found that the $k - \epsilon$ model accurately reproduced the velocity and pressure fields when a fine mesh was used.

In this paper we consider the application of the $k - \epsilon$ model for simulating dispersion near an arctic oil-gathering center. Our primary interest in this specific application is to determine if the numerical model can predict the flow features that control the dispersion of pollutants near buildings. This is significant because the explicit prediction of the flow features at this clustered industrial site will eliminate the large uncertainty associated with Gaussian model parameterization of plume downwash. The computer resources required to run this numerical model are considerable by current standards. Continued rapid advances in computer technology, however, could make this a widely available air quality assessment tool at some future date.

Meteorological and source data collected in field and wind tunnel investigations of GC2 provide the inputs for our numerical model simulations and are the basis for evaluation of model results. A brief description of these databases is presented in the first part of this paper, followed by a description of the numerical model. The results of model simulations are then presented and compared to data collected in the field and wind tunnel studies.

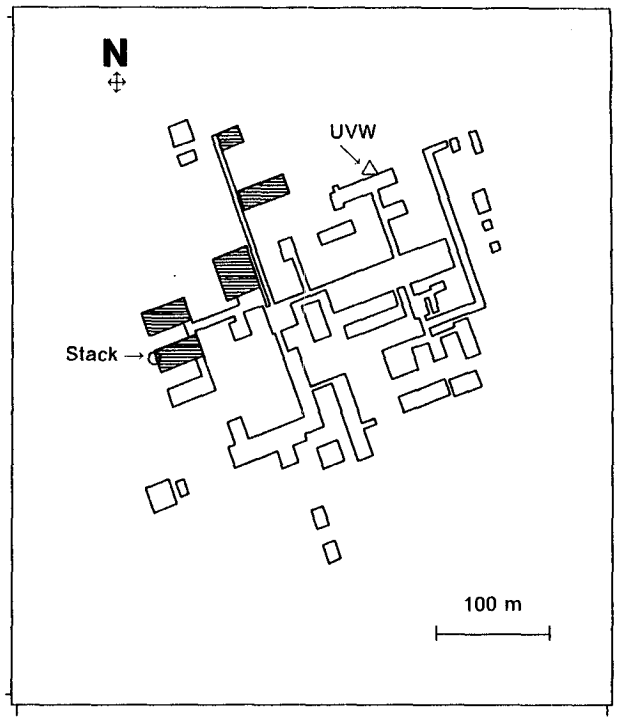

FIG. 1. Map of the Gathering Center 2 complex and turbine stack. Hatched buildings are 20 to 35 m tall, whereas all others are about 20 m.

2. Arctic plume downwash databases

Dispersion near the arctic oil-gathering center, GC2, shown in Fig. 1 has been investigated in field and wind tunnel experiments. The wind tunnel study was conducted by the Radian Corporation and NHC Wind Engineering Inc. (1985) as part of an air quality assessment. The atmospheric dispersion comparability tests recommended by the EPA Fluid Modeling Guideline (Snyder 1981) were conducted prior to this wind tunnel experiment to ensure that the wind, turbulence, and dispersion characteristics in the wind tunnel were similar to those observed in the atmosphere. A surface roughness characteristic of the Alaskan tundra was used to develop the approach boundary-layer profile. The observed dispersion with no buildings present was near the values expected for class D (neutral) in the Pasquill–Gifford (PG) stability classification system. Our arctic field measurements (Guenther and Lamb 1989) suggest that the wind tunnel model provided a reasonable approximation of the wintertime arctic boundary layer.

The 1 to 250 scale model used in the wind tunnel was constructed with building and landscape features extending to 300 m from the center of the facility. The sampling grid consisted of eight downwind rows, perpendicular to wind direction, with up to 12 tracer receptors per row. Up to 48 sample locations were capable of being tested simultaneously. The resulting database contains a total of 24 simulations that include three wind speeds (6, 12, and 24 m s^{-1}) at each of the eight primary wind directions. Three hydrocarbon tracers were used during each run to obtain results from a 33.5 MM Btu $\cdot$ h^{-1} heater, a 4.9 MHP turbine, and a 35 MHP turbine source. We recently used the results of this study to analyze the processes controlling dispersion near buildings and to evaluate the performance of a Gaussian building wake dispersion model (Guenther et al. 1989).

The field study was conducted as the major part of a 3-year program funded by the EPA Cold Climate Research Program to validate and improve current air quality modeling techniques for arctic industrial facilities and has been described by Guenther et al. (1990) and Guenther and Lamb (1989). The area surrounding GC2 is characterized by flat terrain with a very gradual slope ($\approx$0.1%). A surface roughness of 0.03 cm was measured over the open tundra. SF_6 tracer dispersion was investigated during wintertime conditions that include a snow-covered tundra and negligible solar insolation. As a result of the low surface roughness, the vertical wind speed power law exponents were in the range of 0.06 to 0.14 during near neutral conditions and 0.2 to 0.35 during stable conditions. Another feature of the arctic wintertime boundary layer observed during this study was a temperature inversion between

the surface and 10 m and between 300 m and 1 km. This occurred even when wind speeds were greater than 15 m s^{-1}. A lack of surface heating due to the absence of solar insolation is responsible for the very cold tundra surface that creates these inversion layers. The dispersion of pollutants emitted from elevated sources, however, is primarily influenced by the near-neutral layer between 10 and 300 m.

Tracer was released from an operating 35 MHP turbine during east winds (20° to 120°) when wind speed was above 6 m s^{-1}. Lower wind speeds resulted in negligible ground-level concentrations due to the large plume rise. Tracer concentrations were measured by using syringe samplers and continuous tracer analyzers. An infrared (IR) video system provided near-source visualization of the heated plume (see Rickel et al. 1989). Fifteen-minute-average wind speed and direction in the approach flow were measured with a Doppler sounder at 13 heights between 60 and 450 m and with cup anemometers at four heights between 1 and 17 m. Gill propeller UVW (three wind component: u, v, w) anemometers measured the airflow (sampling frequency = 1 Hz) at a height of 33 m directly upwind of the 34-m-high turbine stack and at a height of 2 m within the wake of the GC2 complex. Hourly averaged stack velocity and temperature were measured throughout the study.

3. Numerical model

a. Governing equations

Airflow and thermal dispersion were modeled using an Eulerian, three-dimensional finite difference code, called CELESTE, which was developed at Battelle Pacific Northwest Laboratory and has been applied to a broad range of engineering and geophysical problems (Trent and Eyler 1987). CELESTE solves the time-averaged equations governing continuity, momentum, and energy conservation in the ABL using a semi-implicit, time-marching, elliptic solution method. At each time step the momentum equations are solved explicitly and the pressure equations implicitly. Scalar transport equations for temperature, turbulent kinetic energy, and dissipation are solved using an implicit continuation procedure. The code uses the marker and cell method to define the location of velocity components (on the center of the cell surface) and scalar quantities (at the center of the cell).

The set of equations used in the model are

$$U_{i,i} = 0 \qquad (1),$$

$$\frac{\delta U_i}{\delta t} + U_j U_{i,j} = \frac{1}{\rho_0}[-p,i + \mu U_{i,jj} - \rho g \delta_{3i} - F_i] \quad (2)$$

and

$$\rho_0 c_p\left(\frac{\delta T}{\delta t} + U_j T_{,j}\right) = \kappa T_{,jj} + Q \qquad (3),$$

where U_i is the i velocity component, t is time, ρ is density, p is pressure, μ is an effective viscosity that is the sum of molecular viscosity and an estimated turbulent viscosity (μ_t), $g\delta_{3i}$ is the body force due to gravity (=9.81 m s^{-2}), F_i is the i-direction drag force, c_p is specific heat, T is temperature, κ is an effective thermal conductivity that is the sum of thermal conductivity and an estimated turbulent thermal conductivity (κ_t) and Q is a volumetric heat generation rate. We have used an index notation throughout this paper where an unrepeated index in a term indicates an equation for all three spatial dimensions, a repeated index denotes a term within the equation for each spatial dimension, an unrepeated index following a comma indicates a derivative, and a repeated index after a comma indicates a second derivative. The above equations treat density, ρ_0, as a constant (incompressible flow) except in the body force term, ρg, of the momentum equation, which allows us to simulate a buoyant source. This assumption, known as the Boussinesq approximation, is valid in our domain of interest (the lowest 1 km of the atmosphere) where the variation in ambient density is about 10%. Equation 2 assumes that Coriolis effects are negligible, which is valid in the surface layer, while Eq. (3) assumes that viscous dissipation does not play a significant role in the conservation of energy and can be eliminated from this equation.

A $k-\epsilon$ turbulence model [Eqs. (4)–(7)] is used to close the above system of equations by providing estimates of effective turbulent viscosity and thermal diffusivity. This is accomplished by using transport equations to determine the distribution of turbulent kinetic energy, k,

$$\frac{\delta k}{\delta t} + U_i k_{,i} = \left(\frac{\nu_t}{\sigma_k} k_{,i}\right)_{,i} + \nu_t(U_{i,j} + U_{j,i})U_{i,j} + \beta g_i \frac{\nu_t}{\sigma_t}\rho_{,i} - \epsilon \quad (4)$$

and the dissipation of turbulent kinetic energy, ϵ,

$$\frac{\delta \epsilon}{\delta t} + U_i \epsilon_{,i} = \left(\frac{\nu_t}{\sigma_\epsilon}\epsilon_{,i}\right)_{,i} + c_{1\epsilon}\frac{\epsilon}{k} \times [\nu_t(U_{i,j} + U_{j,i})U_{i,j}] + c_{3\epsilon}\frac{\epsilon}{k}\frac{\nu_t}{\sigma_t} g_i \rho_{,i} - c_{2\epsilon}\frac{\epsilon^2}{k} \quad (5)$$

and then applying relations for turbulent viscosity

$$\nu_t = c_\mu \rho \frac{k^2}{\epsilon} \qquad (6)$$

and a turbulent thermal diffusivity

$$\kappa_t = \frac{\nu_t}{\sigma_t} \qquad (7)$$

where β is the volumetric expansion coefficient and σ_t; σ_ϵ, σ_k, $c_{1\epsilon}$, $c_{2\epsilon}$, $c_{3\epsilon}$, and c_μ are empirical constants. The

values of the constants for the $k-\epsilon$ turbulence closure model are fairly standardized for most engineering applications but are not universal constants for all turbulent flows (Rodi 1980). Detering and Etling (1985) found that the mixing length and velocity profiles produced by the standard $k-\epsilon$ equations and constants did not agree with observed atmospheric profiles (Lettau 1950). They were able to generate more accurate results using

$$(\sigma_t, \sigma_\epsilon, \sigma_k, c_{2\epsilon}, c_{3\epsilon}, c_\mu) = 0.7, 1.3, 1.0, 1.92, 1.44, 0.026) \quad (8)$$

and

$$c_{1\epsilon} = \frac{960 f c_\mu^{3/4} k^{3/2}}{u_* \epsilon} \quad (9)$$

where u_* is friction velocity and f is the Coriolis parameter. In addition to the modifications recommended by Detering and Etling (1985), we simulated a surface roughness (0.03 cm) representative of the arctic tundra by using a value of 0.1 for the constant, E, in the standard engineering equation used to determine the velocity, U, a small distance, z, from a no-slip boundary,

$$U = \frac{u_*}{K} \ln\left(E \frac{u_* z}{\nu}\right) \quad (10),$$

where ν is the kinematic molecular viscosity and K is von Kármán's constant (=0.4). This value of E is two orders of magnitude less than the value (=9.79) based on empirical observations of pipe flow with smooth walls, used in most engineering applications. The computed vertical wind profile shown in Fig. 2 agrees with our observations over the open arctic tundra at heights above 20 m, but slightly overestimates velocities closer to the ground.

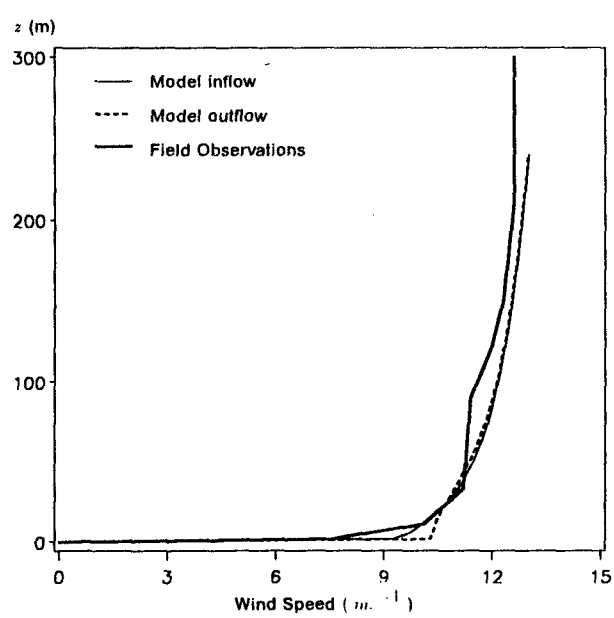

FIG. 2. Vertical logarithmic wind speed profiles for model input, model outflow, and observed over open arctic tundra.

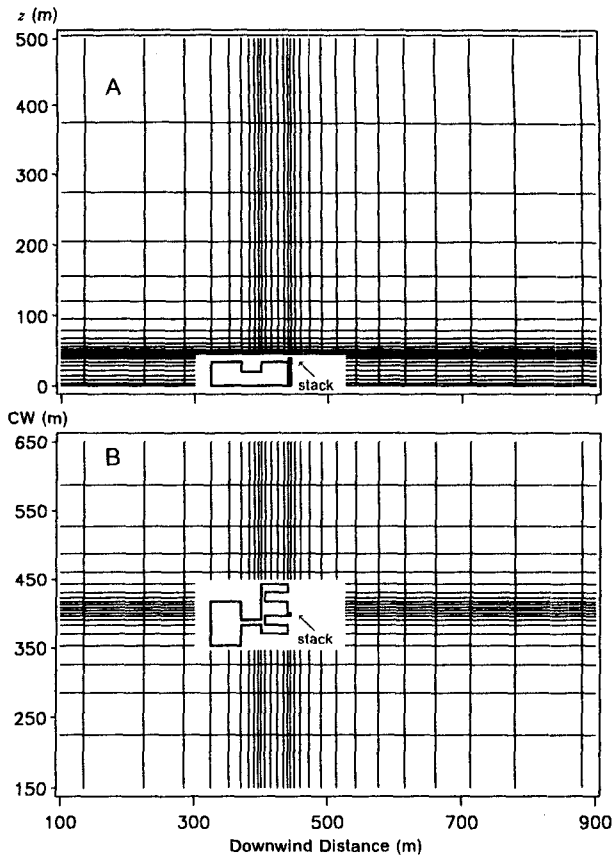

FIG. 3. Spatial resolution of model domain in the vertical (a) and horizontal (b) plan view. Vertical (z) and crosswind (CW) distances are in meters from domain boundaries. Note that only a portion of the 1420 m (downwind) × 947 m (crosswind) × 1625 m (vertical) domain is shown.

b. Model domain and computational requirements

The major features of selected buildings within the GC2 complex were adequately resolved in our modeling domain using the variable mesh Cartesian coordinate system shown in Fig. 3. The vertical grid resolution surrounding the turbine building varied from 3.3 m at the ground and at stack height to 6 m at the center of the building. This provided good resolution for the large gradient near the ground and near the release height. The horizontal grid (both downwind and crosswind directions) was 4 m adjacent to the building and 13 m at a distance of 1 building height (=34 m) downwind or crosswind. This allowed for better resolution of the upwind and downwind recirculation zones. Grid dimensions were gradually increased toward the edges of the domain with the restriction that no cell dimension was more than 50%

greater than that of an adjacent cell. The dimensions of the entire domain were 1420 m (downwind) by 947 m (crosswind) by 1625 m (vertical). In terms of the 34-m building height (H_B), the upwind edge was 10 to 12 H_B from any buildings, the downwind border was 24 to 26 H_B, the side borders were 11 to 14 H_B, and the vertical domain extended to 40 H_B.

Simulations included situations with no buildings, a single building (20 × 40 m) attached to the stack, or an interconnected set of seven buildings covering a 130 × 80 m area. The buildings were oriented to simulate either easterly (70°) or westerly (250°) winds. The simulated approach wind speed at stack height was 12 m s^{-1} with near-neutral thermal stratification. In Table 1 it is shown that these conditions correspond closely to those observed during the field experiments used to evaluate this numerical model.

Turbulent kinetic energy profiles for the inflow boundary conditions were based on the calculations of Detering and Etling (1985). Dissipation profiles were obtained from k and the eddy viscosity determined by Lettau (1950). The outflow boundary was allowed to develop with the simulation. The side and top boundaries were rigid, adiabatic, free-slip boundaries. The velocity components, k, and ϵ within two nodes of the side, top, inflow, and outflow boundaries did not deviate from the initial inflow conditions. This indicates that these boundaries were sufficiently removed from building-wake region and did not significantly influence the results. No-slip boundary conditions were used for the ground and for building surfaces. The 3.66-m diameter turbine stack was modeled with zero-thickness, full-slip walls surrounding a 3.25 × 3.25 m grid cell. Full-slip boundary conditions were used to allow vertical flow through the single cell width of the turbine stack. A constant stack temperature (302°C) and velocity (19 m s^{-1}) typical of field measurements were used as boundary conditions for the grid cells representing the turbine stack.

TABLE 1. Stack, building and meteorological parameters for the field, wind tunnel, and numerical experiments.

Building width	20 m	
Building length	40 m	
Building height	34 m	
Stack height	39.2 m	
Stack cross-sectional area	10.5	(actual)
	10.9	(num. model)

	Field	Wind tunnel	Numerical
Wind speed at 39 m (m s^{-1})	10–14	12	12
Wind Dir. (deg)			
East	60–90	90	70
West	none	270	250
Stack temp. (K)	570–577	450	575
Stack vel. (m s^{-1})	18.8–19.5	20.1	19
Buoy. flux (m^4 s^{-3})	340–370	280	360
Mom. flux (m^4 s^{-2})	540–580	780	560

A convergence criterion of <0.1% change per time step in temperature and velocities at all nodes was applied to all model simulations. The 32 × 28 × 25 grid domain used for the simulations described in this paper required 16 Mbytes of virtual memory and up to 2 × 10^4 CPU seconds on an IBM 3090-300, which has a computational speed of 44 mips (1 × 10^6 instructions per second). A simple cubical building and release stack can be modeled with a 26 × 26 × 16 domain that requires 8 Mbytes of virtual memory and up to 1 × 10^4 CPU seconds. Each of the model simulations assume steady state flow (i.e., boundary conditions did not change with time) which corresponds to the wind tunnel experiments and to the ABL for short (<10 min) time periods. The present code does not allow a nonorthogonal approach flow, which prevents us from simulating wind meander (unsteady flow).

c. *Model sensitivity analysis*

Variation of the turbulence model parameters indicates that the simulated flow patterns were not greatly influenced by our modifications of the turbulence model. Velocities near the ground were the most sensitive of the model output variables, and will be used for comparison in the following discussion. The variable E, used to generate a velocity profile near walls in Eq. (10), is proportional to the roughness length used in atmospheric equations. The standard engineering value of E = 9.79 resulted in velocities near the ground that were about 10% greater than expected for the wintertime arctic atmospheric boundary layer. Reducing E to 0.1, equivalent to the typical wintertime arctic tundra surface roughness of 0.03 cm, results in a 2% decrease in velocity near the ground. A value of E = 0.001 would represent open terrain at a nonarctic site and results in another 2% decrease in velocity near the ground. Our analysis suggests that a slightly more accurate velocity profile can be generated by basing E on surface roughness but the impact on dispersion estimates will be negligible in most cases.

The modifications proposed by Detering and Etling [Eqs. (8) and (9)] resulted in a 10% decrease in the velocities near the ground relative to the standard engineering model that overestimates these velocities. Detering and Etling (1985) selected a value of 960 for the coefficient of the pressure term in the ϵ transport equation [Eq. (9)]. Slight increases in the velocities near the ground (1%–2%) resulted when coefficients of 96 and 9.6 were substituted. By increasing the value of this coefficient to 9600, the velocity near the ground was reduced by 7%, which provided close agreement with observed atmospheric wind profiles. An additional result, however, was an order of magnitude increase in ϵ producing unrealistic ϵ values.

When the grid dimensions were increased to five times greater than those described in section 3b, there was no recirculation cavity present in the model sim-

ulation. Although tests suggest that grid independence was not achieved by the mesh described in section 3b, the computational resources required to gain grid independence were prohibitive. This is a result of the automatic time step procedure that the model uses to ensure stability. A grid Reynolds number of less than one results in an extremely small time step. Dawson (1987) incorporated upwind differencing and a second-order modified MacCormack numerical scheme into an earlier version of the CELESTE code and simulated flow around a hill. The increase in accuracy resulted in a larger recirculation zone on the leeward side of the hill. The use of higher-order numerical schemes, however, results in the same trade-off between accuracy and computational time that occurs with decreasing grid size.

A final sensitivity analysis demonstrates the influence of the simulated buoyancy and momentum fluxes on the model output. Buoyancy and momentum fluxes were both increased 50% by using a 4 × 4 m stack instead of a 3.25 × 3.25 m stack. This resulted in a 6% to 15% increase in plume height depending on downwind distance. Similar increases are predicted by the analytical models of Briggs (10%–20%) and Schulman and Scire (3%–10%). The increased buoyancy also resulted in increases in vertical (1%–3%) and horizontal (1%–5%) dispersion coefficients that are similar to those estimated by Briggs (3%–8% for σ_z and 2%–4% for σ_y). The height dependent Huber–Snyder equations

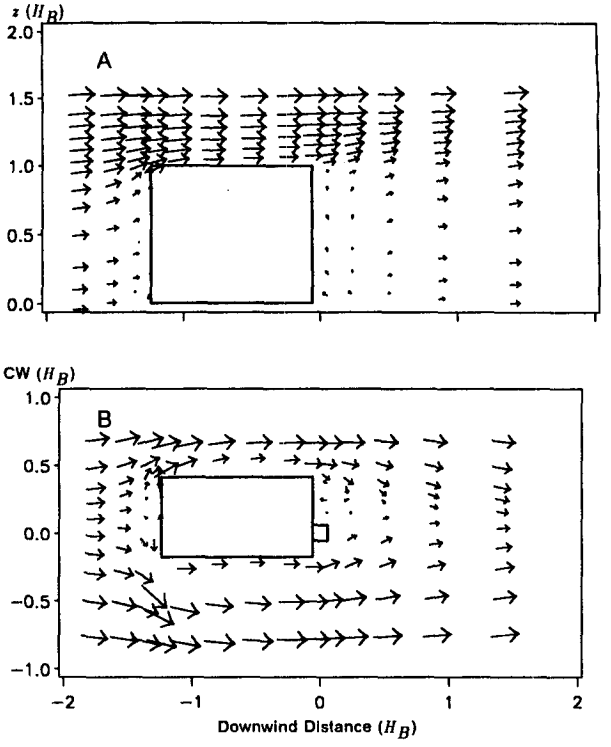

FIG. 5. Velocity vectors for east flow across a single building at a crosswind distance of 0.1 H_B in the vertical (a) and a height of 0.1 H_B in the horizontal (b) plan view. Vertical (z) and crosswind (CW) distances are in building height, H_B (=34 m), from the turbine stack.

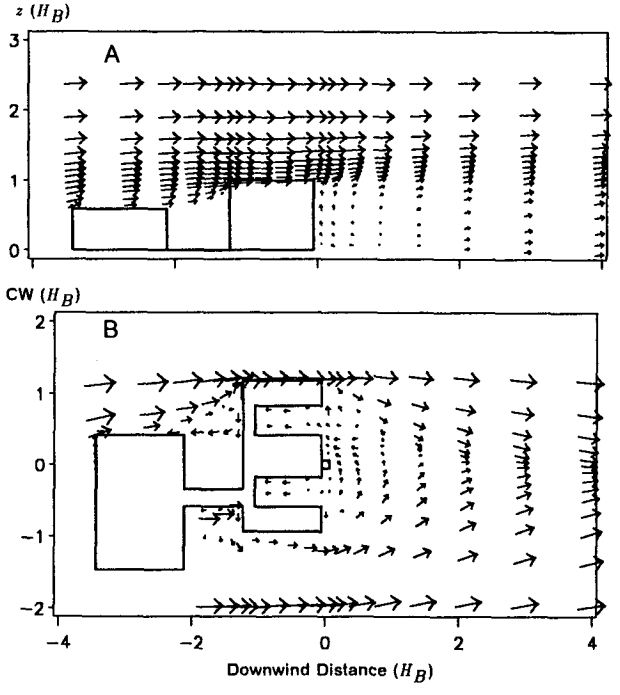

FIG. 4. Velocity vectors for east flow across multiple buildings at a crosswind distance of 0.1 H_B in the vertical (a) and a height of 0.1 H_B in the horizontal (b) plan view. Vertical (z) and crosswind (CW) distances are in building height, H_B (=34 m), from the turbine stack.

(Schulman and Hanna 1986) predict a decrease in σ_z because the higher momentum and buoyancy fluxes place the plume farther above the building wake.

4. Plume downwash simulations

The results described in this section illustrate the ability of CELESTE to calculate dispersion in a building wake. In order to provide a fair evaluation of the numerical model, empirical constants in the model were not adjusted to provide better agreement with field and wind tunnel observations. Figures 4 and 5 show the velocity fields in the vertical and horizontal planes for single and multiple building cases. A recirculation cavity, on upwind and downwind building edges, can be seen in each case. We have defined the recirculation cavity as the region where the downwind velocity is negative or the vertical or crosswind velocity components are a significant component of the total velocity. We found that regardless of whether we defined a "significant component" as 25% or 75%, the cavity height and width simulated by the numerical model is approximately equal to the maximum height and combined width of the simulated set of buildings, respectively. Cavity width increases proportionally as the combined width increases from 0.5 to 3 H_B when additional buildings are included. The downwind length

of the cavity, x_r, measured from the lee face of the building, increases from 0.8 H_B for the single building case to 2 H_B for the multiple building case. Snyder and Lawson (1976) found that x_r ranges from 1.5 H_B for a building width of 0.5 H_B, to 2 H_B for a building width of 2 H_B. Other investigators have measured values of x_r between 2 and 4 H_B (Hosker 1984). Hanna et al. (1982) recommend the following equation for x_r when the streamwise length of the building is larger than the building height:

$$x_r = \frac{1.75\ H_W}{1 + 0.25\ (H_W/H_B)} \qquad (11)$$

where H_W is building width. This equation gives a value of 0.9 H_B for the single building and 3 H_B for the set of buildings, which agrees reasonably well with our modeled results.

The vertical profiles shown in Figs. 6, 7, and 8 demonstrate the impact of the buildings on the flow at several downwind locations. Figure 6 indicates that the velocity defect, $(U_{in} - U)/U_{in}$ where U_{in} is the velocity in the undisturbed approach flow at a given height and U is the velocity at some location downwind, is greater than or equal to 1 at heights below 1 H_B near the buildings. This indicates that recirculation (negative velocities) occurs in this region. The mean velocity defect at a downwind distance of 2 H_B, averaged over heights up to 1.5 H_B, decreases to 0.7 for the multiple building case and 0.3 for the single building case. A velocity defect of 0.6 was observed at a height of 0.1 H_B and a downwind distance of 2 H_B in the field. The mean velocity defect for both single and multiple cases decreases to 0.15 at 10 H_B. The buildings have little impact on the flow beyond 20 H_B downwind where the mean velocity defect is less than 0.05. The addition of more buildings into the modeling domain increases both the size and the strength of the recirculation cavity.

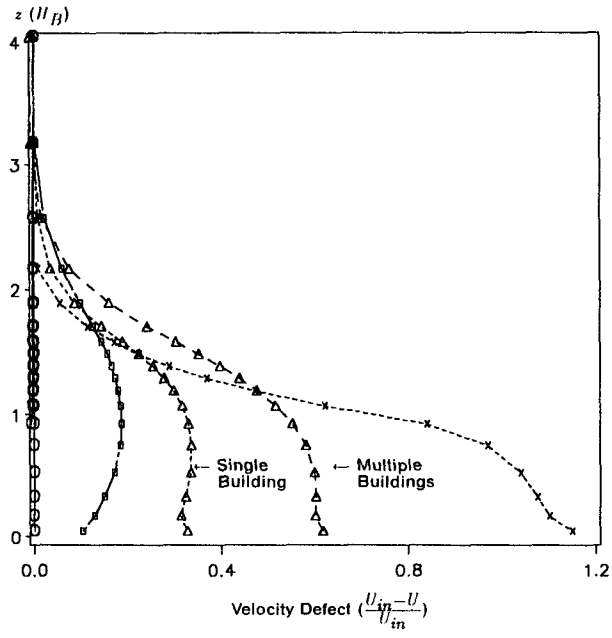

FIG. 6. Vertical velocity defect, $(U_{in} - U)/U_{in}$, where U_{in} is inflow velocity and U is velocity at a given location downwind, profiles computed at 0.15 H_B (×), 3 H_B (△), 10 H_B (●) and 20 H_B (○), downwind of leeward edge. All are for the east wind, multiple buildings case. The single building case at 3 H_B is shown for comparison. Distances are in building height, H_B (=34 m).

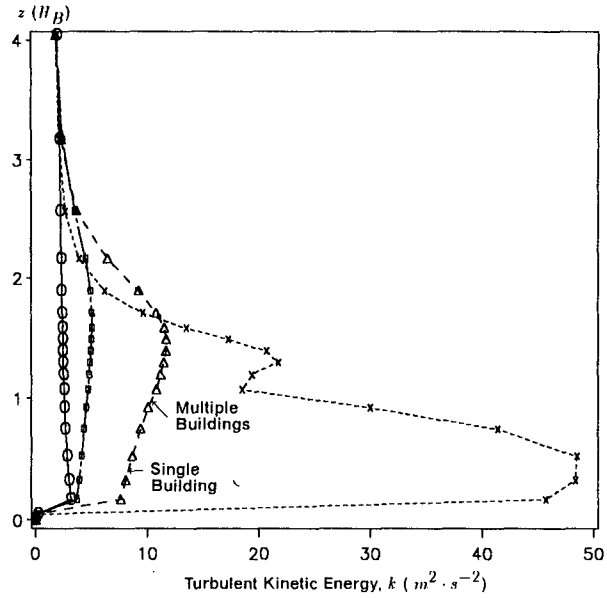

FIG. 7. Vertical turbulent kinetic energy profiles at the inflow (○) and computed at 0.15 H_B (×), 3 H_B (△) and 10 H_B (●) downwind of leeward edge. All are for the east wind, multiple buildings case. The single building case at 3 H_B is shown for comparison. Distances are in building height, H_B (=34 m).

Figure 7 shows the modeled increase in k, relative to the inflow values, downwind of the buildings. Turbulence is near background levels at heights above 2.5 H_B and downwind distances greater than 10 H_B. An increase in k from 0.97 $m^2\ s^{-2}$ outside of the building wake to 3.9 $m^2\ s^{-2}$ at 2 H_B downwind was measured with UVW anemometers at a height of 0.06 H_B in the field. The modeled value of k increased from 2.5 $m^2\ s^{-2}$ in the approach flow to 8.6 $m^2\ s^{-2}$ at 2 H_B downwind of the building at a height of 0.17 H_B. The factor of 3.4 to 3.9 increase in k calculated by the model for all heights between 0.1 and 1 H_B agrees closely with the factor of 4 increase observed in the field. A large decrease in the modeled value of k at a height of 0.05 H_B (the first node) occurs whether buildings are present or not. This result and the factor of 20 increase in k at a downwind distance of 0.15 H_B (shown in Fig. 7) are both unrealistic. These inaccurate estimates of k near solid boundaries may be the result of assumptions in the $k - \epsilon$ model such as the use of an eddy viscosity.

The increase in modeled values of ϵ in the building wake is shown in Fig. 8. Perturbations in the ϵ field extend up to a height of 2.5 H_B and downwind to a

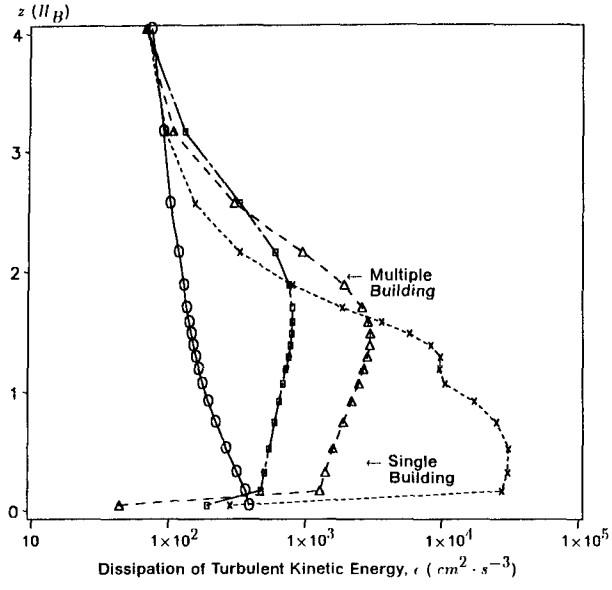

FIG. 8. Vertical dissipation profiles at the inflow (O) and computed at 0.15 H_B (×), 3 H_B (△) and 10 H_B (●) downwind of leeward edge. All are for the east wind, multiple buildings case. The single building case at 3 H_B is shown for comparison. Distances are in building height, H_B (=34 m).

distance of 10 H_B. Modeled values of ϵ at a height 0.17 H_B increase from 327 cm^2 s^{-3} in the approach flow to 1500 cm^2 s^{-3} at 2 H_B. Values of ϵ calculated from velocity component spectra measured at a height of 0.07 H_B in the field (see Guenther and Lamb 1989) increase from 30 cm^2 s^{-3} to 200 cm^2 s^{-3}. Values of k and ϵ computed for the single building case are within 15% (higher below 1 H_B and lower above 1 H_B) of the results for the multiple building case. The turbulent viscosity, which is dependent on both k and ϵ, at a height of 0.5 H_B is increased by 45% at downwind distances of up to 3 H_B and by 15% out to 10 H_B downwind of multiple buildings. A single building results in increases of 30% out to 3 H_B and 10% out to 10 H_B.

The vertical transport of the plume centroid with downwind distance is shown for three east wind simulations in Fig. 9. The plume rise calculated by CELESTE with no buildings present is less than that estimated by the analytical plume rise equations developed by Briggs (1984) and the integral equations of Petersen and Ratcliff (1988). The lowered plume rise could be the result of the inability of the buoyancy terms used in the $k-\epsilon$ model to account for buoyancy effects adequately (Hossain and Rodi 1982). The plume rise computed by CELESTE decreases as buildings are added to the simulation. This is the result of entrainment into the recirculation cavity and increased turbulent diffusion. The downwashed plume rise computed by CELESTE is similar to values estimated by

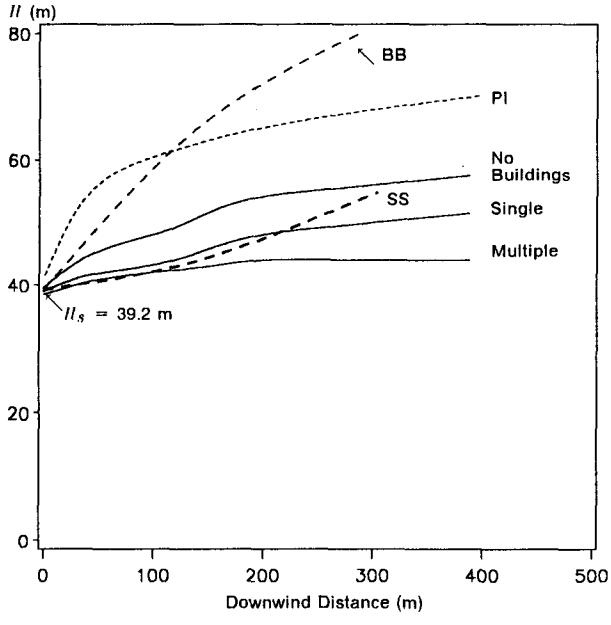

FIG. 9. Plume height (m) as a function of downwind distance (m) simulated by CELESTE for east winds (solid lines). Estimates by the Briggs (BB), Petersen integral (PI), and Schulman and Scire downwashed (SS) plume rise equations for the same conditions are shown for reference.

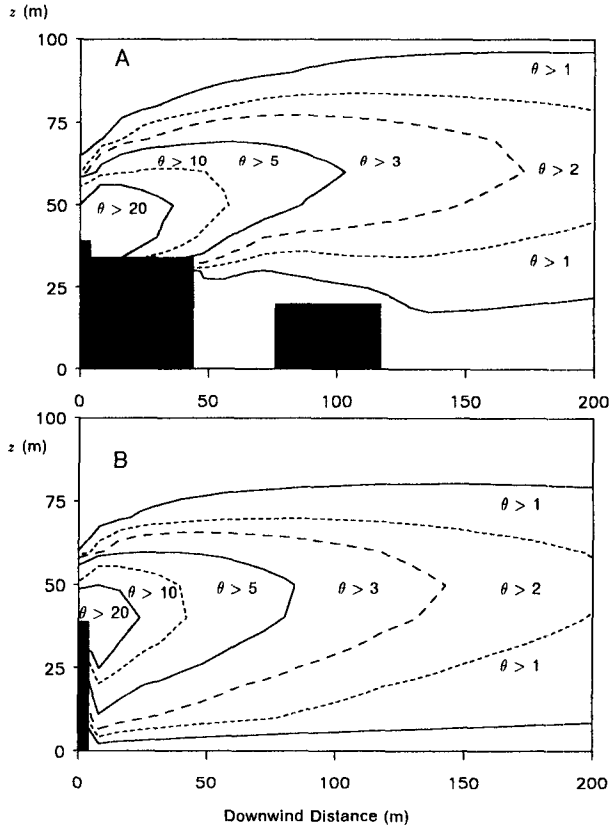

FIG. 10. Vertical thermal plume isopleths from a 35 MHP turbine for west (a) and east (b) winds with multiple buildings. The term θ is the temperature (°C) increase over ambient. Vertical (z) and crosswind (CW) distances are in meters.

downwashed plume rise equations (Schulman and Hanna 1986). Observed plume rise in the field (out to 15 m downwind) indicates that the downwashed plume estimates are a factor of 5 too low. It is possible, however, that plume rise at longer downwind distances is lowered by entrainment into the recirculation cavity.

The wind tunnel observations demonstrate that wind directions that are offset 180° (e.g., east and west winds), and which have the same projected building widths, can result in a factor of 2 difference in ground-level centerline concentration. This change is presumably caused by differences in the position of the stack relative to the buildings for the two wind directions. The thermal isopleths shown in Fig. 10 demonstrate that the plume rise and vertical dispersion computed by the numerical model are different for the west (stack on the upwind building edge) and east (stack on the downwind building edge) wind cases with multiple buildings. Since differences are also seen, but are not as great, for west and east wind flow across a single building, it is likely that this is the result of the placement of the stack relative to the attached building, in addition to the influence of upwind and downwind buildings. Another probable factor is that the resolution was not sufficient for a downwind recirculation zone to be formed for west winds and that this resulted in a lack of plume downwash. In Fig. 3 it is shown that the building farthest from the stack (downwind for the west wind case) is in a zone with larger grid dimensions than those surrounding the stack.

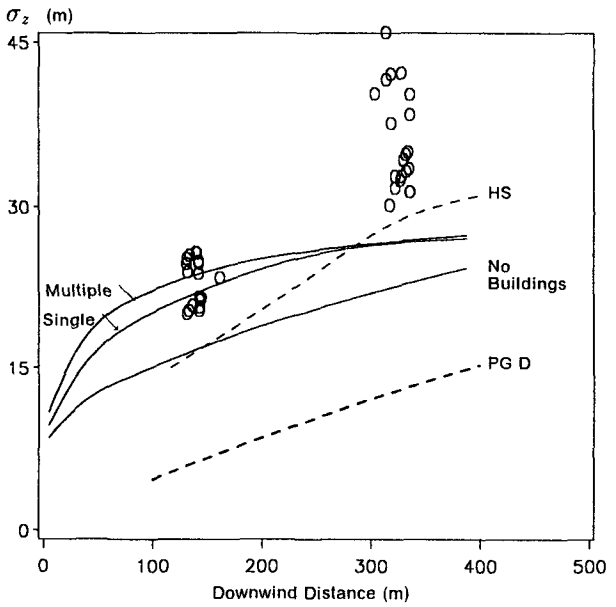

FIG. 11. Vertical plume width, σ_z (m), as a function of downwind distance (m) simulated by CELESTE for east winds. Field tracer observations (Guenther et al. 1990) are indicated by (O). The Huber–Snyder building wake dispersion equation (HS) and the Pasquill–Gifford near-neutral dispersion equation (PG D) estimates are shown for comparison.

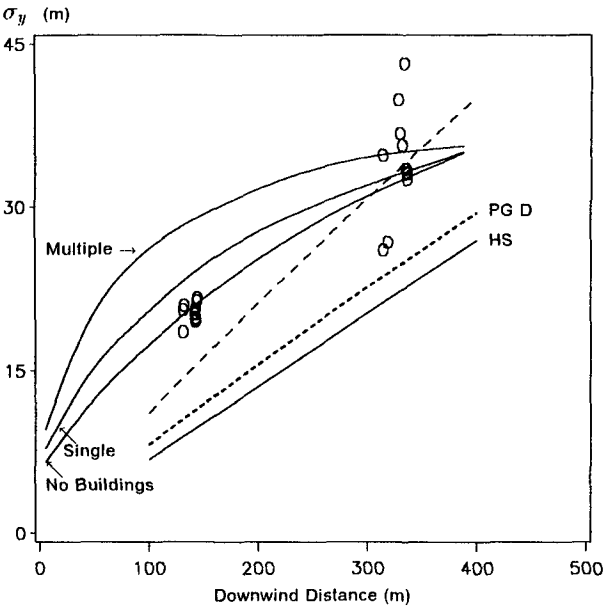

FIG. 12. Horizontal plume width, σ_y (m), as a function of downwind distance (m) simulated by CELESTE for east winds. Field tracer observations (Guenther et al. 1989b) are indicated by (O). Estimates predicted by the Huber–Snyder building wake dispersion equation (HS) and the Pasquill–Gifford near-neutral dispersion equation (PG D) are shown for comparison. Huber and Snyder (1982) recommend using the PG estimates if they exceed the HS values.

The vertical distribution of west and east wind thermal plumes is illustrated in Fig. 10. These distributions can be described by defining a characteristic plume volume as the central 68% of the total plume. The radius of this volume in the vertical, (σ_z), and horizontal, (σ_y), directions represents characteristic plume dimensions that are equivalent to standard Gaussian model coefficients. Huber and Snyder (1982) have used the results of wind tunnel experiments to develop some general algorithms to predict σ_y and σ_z downwind of buildings. Figures 11 and 12 demonstrate that these equations underestimate field tracer measurements of dispersion measured with east winds at the arctic oil-gathering center. This is at least partly because the Huber–Snyder and Pasquill–Gifford equations do not account for buoyancy-induced dispersion. The lateral dispersion observed in the wind tunnel was also less than that observed in the field, which is expected due to the absence of wind meander in the wind tunnel, but estimates of vertical dispersion are in agreement. The values of σ_z shown in Fig. 11 indicate that the numerical model predicts that σ_z increases as buildings are added to the simulation. The building-enhanced σ_z calculated from the model results are within the range of σ_z estimated from field observations at 3 H_B but are less than observed at 10 H_B. The numerical model estimates of σ_y displayed in Fig. 12 also demonstrate building-enhanced lateral dispersion, which is in agreement with field observations at downwind dis-

tances of less than 3 H_B. The absence of increased dispersion beyond 3 H_B is probably the result of poor resolution at the plume edges at these larger downwind distances. When no buildings are present, the model computes a much greater σ_z and σ_y than would be expected for neutral conditions based on the Pasquill–Gifford estimates for nonbuoyant, open-terrain dispersion. The Pasquill–Gifford estimates do not account for buoyancy-induced and stack-enhanced dispersion, which may explain the difference between field observations and model values of σ_y and σ_z.

The results of these model simulations indicate that dispersion from a short turbine stack within an arctic industrial complex is significantly influenced by building-generated dispersion and by entrainment into a recirculation cavity. The dimensions of the recirculation cavity and the thermal plume simulated by the model agree fairly well with field and wind tunnel observations.

5. Conclusions

In this paper we have described a numerical model that is capable of simulating non-Gaussian dispersion in a building wake. The model is a three-dimensional, Cartesian coordinate, finite difference code that solves the nonhydrostatic, time-averaged equations for the conservation of continuity, momentum, and energy. The code uses a modified form of the standard first-order, two-equation ($k - \epsilon$) engineering turbulence closure model. The results of numerical model simulations of dispersion from a buoyant source located in the wake of an arctic industrial complex were presented and compared with field and wind tunnel observations. The model was able to simulate the major features observed in the field. This included a near-wake region (out to 1–2 H_B) containing a pronounced recirculation cavity and greatly increased turbulence and a far wake region (from 2–10 H_B) where reduced velocities and slightly increased turbulence levels occurred. Decreased plume rise and increased lateral and vertical plume width were observed with the addition of buildings to the numerical model. This is in agreement with field and wind tunnel observations.

The numerical investigation described in this paper demonstrates that realistic plume downwash and enhanced dispersion can be simulated with a $k - \epsilon$ model. Pollutant dispersion can be simulated directly by adding an equation for turbulent mass transport to the set of equations solved by CELESTE. This would provide a tool that could be used to estimate ground-level pollutant concentrations when Gaussian modeling techniques are inappropriate. Before this objective can be realized, methods of increasing accuracy (e.g., modification of buoyancy and other terms in the turbulence equation, and increasing resolution while maintaining a reasonable computational cost) must be investigated further. Only when the pollutant concentrations estimated by this numerical model represent a significant improvement over Gaussian model predictions and when the model's resource requirements and expense are considerably less than that associated with field and wind tunnel experiments, will this technique provide the regulatory assessment tool that is currently needed.

Acknowledgments. This work was funded by the U.S. Environmental Protection Agency (CR 812775-01) through the EPA Cold Climate Research program. The contents of this paper do not necessarily reflect the views and policies of the agency, nor does mention of trade names or commercial products constitute endorsement or recommendations for use. Computation time on the IBM 3090-300 at Washington State University was provided by WSU Systems and Computing. The authors would like to thank Paul Dawson for his assistance in running the model simulations and Don Trent of Battelle Pacific Northwest Laboratories for supplying the CELESTE code. We would also like to thank Peter Finkelstein of the EPA for his support and guidance as Project Officer.

REFERENCES

Briggs, G. A., 1984: Plume rise and buoyancy effects. *Atmospheric Science and Power Production,* D. Randerson, Ed., DOE/TIC-27601. Technical Information Center.

Dawson, P. J., 1987: A numerical model to simulate the atmospheric transport and diffusion of pollutants over complex terrain. Ph.D. thesis. Washington State University.

Detering, H. W., and D. Etling, 1985: Application of the $E - \epsilon$ turbulence model to the atmospheric boundary layer. *Bound.-Layer Meteor.,* **33,** 113–133.

Guenther, A. B., and B. K. Lamb, 1989: Atmospheric dispersion in the Arctic: Wintertime boundary-layer measurements. *Bound.-Layer Meteor.,* **49,** 339–366.

——, —— and R. Petersen 1989a: Modeling of plume downwash and enhanced diffusion near buildings: Comparison to wind tunnel observations for an arctic industrial site. *J. Appl. Meteor.,* **28,** 343–353.

——, ——, and E. Allwine, 1990: Field tracer observations and model evaluations of plume downwash and dispersion at an arctic industrial site. *Atmos. Environ.,* in press.

Lettau, H., 1950: A re-examination of the Liepzig Wind Profile considering some relations between wind and turbulence in the friction layer. *Tellus,* **2,** 125–129.

Hanna, S. R., G. A. Briggs and R. P. Hosker, 1982: *Handbook on Atmospheric Diffusion* DOE/TIC-11223. National Technical Information Center.

Hossain, M. S., and W. Rodi, 1982: A turbulence model for buoyant flows and its application to vertical buoyant jets. *Turbulent Buoyant Jets and Plumes,* W. Rodi, Ed., Pergamon, 184 pp.

Hosker, R. P., Jr., 1984: Flow and diffusion near obstacles. *Atmospheric Science and Power Production,* D. Randerson, Ed., DOE/TIC-27601. National Technical Information Center.

Huber, A. H., and W. H. Snyder, 1982: Wind tunnel investigation of the effects of a rectangular-shaped building on dispersion of effluents from short adjacent stacks. *Atmos. Environ.,* **17,** 2837–2848.

Mathews, E. H., 1987: Prediction of the wind-generated pressure distribution around buildings. *J. Wind Eng. Ind. Aerodyn.,* **25,** 219–228.

Muramaki, S., and A. Mochida, 1988: 3-D numerical simulation of airflow around a cubic model by means of the $k - \epsilon$ model. *J. Wind Eng. Ind. Aerodyn.* **31,** 283–303.

——, —— and K. Hibi, 1987: Numerical prediction of velocity and pressure field around building models. Preprints, *7th Conf. on Wind Engineering,* Aachen, Vol. 2, 31–40.

Paterson, D., and C. Alpelt, 1986: Computation of wind flows over three-dimensional buildings. *J. Wind Eng. Ind. Aerodyn.* **24,** 192–213.

Petersen, R., and M. Ratcliff, 1988: Industrial Source Complex model with integral plume rise and dispersion enhancement (ISCIPRA) user's guide, 2nd ed., Vol. I. CPP project 87-S-0187, American Petroleum Institute, Washington, DC.

Radian Corporation, and NHC-Wind Engineering, Inc., 1985: The North Slope air quality compliance verification project. Radian DCN 85-242-039-10-01, Houston.

Rickel, C., B. Lamb, A. Guenther and E. Allwine, 1989: An infrared method for plume rise visualization and measurement. *Atmos. Environ.,* submitted.

Rodi, W., 1980: Turbulence models for environmental problems. *Prediction Methods for Turbulent Flows.* W. Kollman, Ed., Hemisphere, 468 pp.

Schulman, L. L., and S. R. Hanna, 1986: Evaluation of downwash modifications to the Industrial Source Complex model. *J. Air Pollut. Control Assoc.,* **36,** 258–264.

Snyder, W. H., 1981: Guidelines for fluid modeling of atmospheric diffusion. EPA-600/8-81-009, Research Triangle Park, NC.

——, and R. E. Lawson, Jr., 1976: Determination of a necessary height for a stack close to a building, *Atmos. Environ.,* **10,** 683–691.

Trent, D. S., and L. L. Eyler, 1987: CELESTE: A three-dimensional time-dependent computer program for fluid dynamic analysis. Numerical methods and input instructions, Battelle, Pacific Northwest Laboratories.